Vilnius University

Physics faculty

Institute of Applied Electrodynamics and Telecommunication

Kipras Gudeliauskas

Noise spectroscopy of heterostructures with a gallium oxide layer

Master's final thesis

Electronics and telecommunications technology program

Student	Kipras Gudeliauskas
Approved	2026-05-22
Academic supervisor	doc. Sandra Pralgauskaitė
Reviewer	prof. Irmantas Kašalynas
Institute director	prof. Robertas Grigalaitis

Vilnius 2026

Vilniaus Universitetas

Fizikos fakultetas

Taikomosios elektrodinamikos ir telekomunikacijų institutas

Kipras Gudeliauskas

Įvairialyčių darinių su galio oksido sluoksniu triukšminė spektroskopija

Magistrantūros studijų baigiamasis darbas

Elektronikos ir telekomunikacijos technologijų programa

Studentas	Kipras Gudeliauskas
Leista ginti	2026-05-22
Darbo vadovė	doc. Sandra Pralgauskaitė
Recenzentas	prof. Irmantas Kašalynas
Instituto direktorius	prof. Robertas Grigalaitis

Vilnius 2026

Table of Contents

Introduction

Gallium oxide β-Ga_2O_3 is a relatively new and promising ultra-wide bandgap semiconductor that has applications in high-voltage electronics. It has a large bandgap and a high critical electric field. However, its low thermal conductivity and electrically active defects limits gallium oxides applications [1][2][3]. Low frequency noise spectroscopy is a great tool for investigating the quality of these semiconductor materials [4].

Studies have shown that in β-Ga_2O_3 nanoelectronics devices that had increased their cross section changed the noise spectra from $1/f$ to spectra with stronger Lorentzian components. Which would suggest a shift from surface/interface fluctuations to discrete bulk-related centers [5]. In β-Ga_2O_3 FinFETs, a $1/f$ spectrum was suggested to come from carrier capture and emission in an interface between β-Ga_2O_3/Al_2O_3 [6]. MOVPE-grown β-Ga_2O_3 layers and $(Al,Ga)_2O_3$ Schottky barrier diodes exhibited $1/f$ spectra together with Lorentzian components that indicate discrete deep or interface-related traps [7][8]. The simultaneous appearance of $1/f^{\alpha}$ noise together with Lorentzian generation-recombination (g-r) components imply the existence of discrete traps with different characteristic relaxation times.

The goal of this work is to find out origins of electrical fluctuations in the heterostructures with a Ga_2O_3 layer and clear up their impact on the charge carrier transport mechanisms in such structures.

This work is a continuation of a previous master's research work: Noise spectroscopy of gallium oxide layers, Kipras Gudeliauskas, Vilnius University, 2026.

The results of this research will be presented at the International Conference on Unsolved Problems of Noise (UPoN 2026); they are also planned to be included in a scientific publication.

1. Literature overview

1.1 Gallium oxide semiconductor layers

Gallium oxide Ga_2O_3 has emerged as a prominent ultra-wide bandgap semiconductor, that have a bandgap of $\sim 4{,}8 - 4{,}9$ eV and possess a very high critical electric field of about ~8 MV/cm. These properties exceed other more traditional semiconductors like SiC and GaN, allowing Ga_2O_3 devices to handle higher voltages in smaller dimensions with greater efficiency [1]. Ga_2O_3 crystallizes in five polymorphs (α, β, γ, δ, ε), but β-Ga_2O_3 is the most thermodynamically stable phase at ambient conditions [2]. The wide bandgap of β-Ga_2O_3 not only grants it a high breakdown field but also makes it transparent to visible light when it is suitably doped [2]. This transparency and its high electrical conductivity give Ga_2O_3 an advantage in optoelectronic applications over narrower bandgap materials [2].

From an electronic perspective, Ga_2O_3 is suitable for power electronics devices, owing to its combination of wide bandgap and attainable doping densities. Single-crystal bulk β-Ga_2O_3 can be grown from melt, yielding large-area and low-cost substrates [1]. This ready availability of native substrates and epitaxial layers is a significant advantage for device fabrication, distinguishing Ga_2O_3 from GaN and SiC which rely on more expensive or lattice-mismatched substrates [1]. Ga_2O_3 has relatively low thermal conductivity, which is about $0{,}2\ \mathrm{W/cm \cdot K}$ [3]. These issues impose limits on device cooling. Despite these challenges, the ultra-wide bandgap and materials advantages of Ga_2O_3 position it as a very promising semiconductor for next-generation high-voltage electronics and deep-UV optoelectronics.

1.1.1 Ga_2O_3 layer applications

Beyond transistors, Ga_2O_3's unique material properties lend themselves to a variety of device applications. Two prominent examples are solar-blind photodetectors in the deep ultraviolet (DUV) spectrum and Schottky barrier diodes for power rectification. In each case, Ga_2O_3 has demonstrated noteworthy performance, leveraging its wide bandgap and strong electrical breakdown capability.

Ga_2O_3's bandgap of ~4,9 eV corresponds to a cut-off wavelength of roughly 250 nm, meaning it is inherently solar-blind (blind to wavelengths longer than the UVA/UVB range). This makes Ga_2O_3 an ideal semiconductor for DUV photodetectors, which are sensors that selectively detect UV-C radiation (λ ≈ 200-280 nm) while being insensitive to visible light. Traditional solar-blind detectors have used expensive materials like MgF_2 or complex multilayer filters to achieve spectral selectivity, but Ga_2O_3 offers intrinsic selectivity due to its bandgap. Research over the past decade has produced various Ga_2O_3 photodetector architectures: thin-film photoconductors, metal-semiconductor-metal photodiodes, Schottky photodiodes, and heterojunction photodiodes.

One highlight is the development of zero-bias Ga_2O_3 photodetectors reported a zero-power deep-UV photodetector based on a β-Ga_2O_3/Nb-doped $SrTiO_3$ (NSTO) heterojunction, which operates as a self-biased diode. Under DUV illumination, the Ga_2O_3 junction generates a photocurrent without any external bias due to the built-in potential that separates photogenerated electron-hole pairs. This device showed fast photoresponse and a photocurrent to dark current ratio of ~20 at zero bias under modest UV illumination [9]. The mechanism was attributed to the built-in electric field at the heterojunction that drives carriers, meaning the device consumes no power in standby, an attractive feature for remote or low-power sensor systems.

Schottky barrier diodes are typically a simpler structure but are a fundamental component for power conversion. The wide bandgap of Ga_2O_3 allows them to achieve extremely high reverse breakdown voltages with relatively low leakage currents. In addition, Ga_2O_3 can be doped n-type to high levels, yielding low forward resistance. These characteristics position Ga_2O_3 Schottky barrier diodes to outperform Si and approach or exceed SiC/GaN for certain voltage ranges [10].

1.2 Noise in electronic devices

Noise refers to random electrical fluctuations or deviations from the average value of a particular quantity, such as electrical current or voltage. Electrical noise manifests in all electronic devices and systems. Noise arises from various microscopic processes and can be caused by thermal motion of charge carriers, the discrete nature of charge carriers, or parameter instabilities in electronic devices [4]. The measured noise typically consists of several noise components corresponding to different noise generation mechanisms. At low frequencies, in addition to thermal and shot noise, additional noise components appear - generation-recombination and $1/f$ noise - which serve as sensitive indicators of electronic device quality and reliability. Higher device noise levels are generally associated with poorer performance [4].

1.2.1 Thermal Noise

Thermal noise is the random voltage or current produced by the thermal agitation of charge carriers in any resistive element. It exists even in the scenario where there is no net current, whenever a conductor or resistor is at nonzero temperature. This Johnson-Nyquist noise was first measured by J. B. Johnson in 1928, and Harry Nyquist immediately provided a theoretical basis using thermodynamics [11][12]. Nyquist showed that in thermal equilibrium the mean-square noise voltage across a resistor R in a bandwidth Δf at temperature T is

$$\overline{V_{\mathrm{RMS}}^2} = 4k_{\mathrm{B}}TR\Delta f \tag{1.3}$$

where k_{B} is Boltzmann's constant. Equivalently, the one-sided power spectral density of the voltage is flat or sometimes referred to as white and given by

$$S_V(f) = 4k_{\mathrm{B}}TR. \tag{1.4}$$

These formulas imply that thermal noise increases with temperature and resistance which is totally independent of any applied bias [4]. Nyquist's derivation relates this to the fluctuation-dissipation theorem, viewing the resistor as in equilibrium with blackbody radiation modes. Thermal noise is universal for every resistor and electric device that generates this type of noise, setting a fundamental noise floor in amplifiers and circuits. In semiconductors, any resistance contributes to thermal noise. For example, a 1 kΩ resistor at 300 K has $\sqrt{\overline{V^2}} \approx 1$ μV over a 20 kHz bandwidth. Thermal noise thus limits the precision of analog-to-digital converters and low-noise amplifiers. In practical applications the voltage noise spectral density is used and denoted as S_V.

1.2.2 Shot noise

Shot noise arises from the discrete, quantized nature of electric charge: when a DC current flows because individual electrons or holes cross a potential barrier, the arrival times fluctuate randomly. Walter Schottky first identified this noise in vacuum tubes in 1918, coining the term "shot" noise [12]. Shot noise manifests as a white noise current with power proportional to the average current. Under the assumption of independent arrivals, the low-frequency current spectral density is given by the Schottky formula [9]:

$$S_{\mathrm{I}}(f) = 2eI, \tag{1.5}$$

where e is the carrier charge and I is the DC current. Equivalently, in a device with resistance R, the voltage noise spectral density is $S_V = 2eIR^2$. This result was first observed in Schottky's vacuum-tube experiments, who showed the noise is "absolutely white with mean power proportional to the average current" [14].

Physically, shot noise is Gaussian (for large numbers of carriers) and grows with current: the noise current over a bandwidth B has rms value $i_{\mathrm{rms}} = \sqrt{2eIB}$. This can be written in noise density form $i_{\mathrm{n}} = \sqrt{2eI}$ [9]. Examples of this noise appears in p–n junctions, Schottky diodes and photodiodes. In high-speed or high-frequency electronics, shot noise sets the minimum noise level at frequencies above the corner where $1/f$ noise subsides [15].

1.2.3 Generation recombination noise

Generation recombination noise or G-R noise is specific to semiconductors and arises from random fluctuations in the number of free carriers due to generation and recombination events when electrons are transitioning between bands or trapped states. This noise was first experimentally observed in semiconductor crystals around 1951, with the term "G-R noise" introduced a few years later [11]. Theoretical models treat the semiconductor as a system of energy levels (bands and traps) with carriers being randomly captured and emitted. The simplest model is a two-level system with carrier lifetime τ. In such a model, the fluctuation $\Delta N(t)$ in the number of electrons has a Lorentzian spectrum [16]:

$$S_{\mathrm{N}}(f) \propto \frac{4(\Delta N)^2\tau}{1 + (2\pi f\tau)^2}, \tag{1.6}$$

that entails that the G-R noise spectrum drops off above the characteristic frequency $f_c = 1/2\pi\tau$. In practice, the current or resistance noise due to G-R processes also show a Lorentzian dependence on frequency. G-R noise adds excess noise that is above thermal noise and forms a flat "plateau" at low frequencies and decays above the characteristic frequency [16].

A commonly used expression for the excess current noise spectrum in a biased semiconductor is:

$$S_{\mathrm{I}}(f) = \frac{A}{1 + (2\pi f\tau)^2}, \tag{1.7}$$

where A is related to the variance of number fluctuations and τ the recombination lifetime. These Lorentzian G–R contributions can often be separated from $1/f$ noise by plotting $S(f) \times f$ from

f, which highlights a peak around $1/2\pi\tau$ [16]. Generation–recombination noise is vital in many semiconductor devices, particularly at intermediate frequencies below 1 MHz. For example, in p-n junction diodes or photoconductors, traps or defect levels in the bandgap can produce G-R noise. The magnitude of g-r noise depends on temperature, bias and trap densities. In communications and sensor systems, understanding G-R noise is essential for understanding flicker noise.

1.2.4 Flicker $1/f$ noise

Flicker noise, or 1/f noise, is a generic low-frequency noise with a power spectral density approximately proportional to $1/f^{\alpha}$. It was first noticed in vacuum-tube amplifiers: J. B. Johnson observed an unexplained excess noise at low frequencies in tube circuits, and W. Schottky later attempted a theory [12][13]. Flicker noise has since been found ubiquitous in electronic materials and devices. In semiconductors, it often arises from a superposition of many G-R processes or mobility fluctuations and is linked to defects and traps. Today it is empirically described by Hooge's formula or similar laws [4][17]:

$$S_I(f) = \frac{\alpha_{\mathrm{H}} I^2}{Nf}, \tag{1.8}$$

where N is the effective number of free carriers and α_{H} is the "Hooge parameter" which is an empirical constant. Equivalently, device noise is often parametrized as $S_I \propto I^2/f$.

Flicker noise has a spectrum proportional to $1/f$. In devices, this noise is associated with "random fluctuations in current due to defects in semiconductor materials". It is present in essentially all transistors and many resistors. The measured noise voltage in circuits often shows a proportionality $S_U \propto 1/f$ at low frequencies, transitioning to white noise at higher f [10]. Typical corner frequencies range from sub-hertz to a few kHz, depending on device and operating point. Despite decades of study, flicker noise lacks a single universal theory. The origins of flicker noise are treated statistically. But the main result is clear, flicker noise is dominant at low frequencies and increases with DC current. Because it stems from microscopic defects, improving material quality and device design can reduce flicker noise [4].

Another theory describing $1/f$ noise is widely agreed upon that the main cause of flicker noise in semiconductors would be the superposition of generation-recombination spectra [17]:

$$\frac{S_U}{U^2} = \sum_l \frac{a_l \tau_l}{1 + \omega^2 \tau_l^2}, \qquad (1.9)$$

where a_l is a dimensionless parameter that describes the magnitude of noise with relaxation time t_l [13].

1.2.5 Low-frequency noise in Gallium oxide layers as means to test quality

Understanding and mitigating electronic noise is crucial for any semiconductor device, and Ga_2O_3 is no exception. Low-frequency noise that consists of $1/f$ flicker noise or generation-recombination noise provides a sensitive window into the trap states and defects in Ga_2O_3 materials and interfaces. Several recent experimental studies have characterized low frequency noise in Ga_2O_3 thin films and transistors, revealing the nature of trap centers and their dynamics in β-Ga_2O_3 nanowire, FET devices of varying cross-sectional size [5]. They found that as the nanowire diameter increased, the noise spectrum evolved from a pure $1/f$ form to a combination of $1/f$ and $1/f^2$ components [4]. In narrow ~80 nm wires, the noise was predominantly $1/f$, indicative of a broad distribution of many small traps. In thicker ~200 nm wires, distinct Lorentzian $1/f^2$ bulges appeared, signaling the presence of discrete trap centers or trap clusters [5]. The interpretation was that shallow surface/ interface traps with a wide range of time constants contribute the $1/f$ background, whereas deeplevel traps in the nanowire bulk produce g-r noise components [5]. Increasing the bias on these nanowire devices accentuated the $1/f^2$ Lorentzian components and shifted them to lower frequencies [5]. This study highlights that surface traps compared to bulk traps in Ga_2O_3 can be distinguished via low frequency noise analysis, and that device scaling may lower noise by reducing bulk trap volume.

Other studies focused on low-frequency noise in a β-Ga_2O_3 FinFET with an Al_2O_3 gate dielectric, specifically to investigate how oxide traps are distributed and how they change under bias stress [6]. By carefully measuring the power spectral density of drain current fluctuations, they were able to extract the spatial profile of traps in the gate oxide. The noise spectrum followed a $1/f$ shape, consistent with carrier number fluctuation due to trap capture and emission at the β-Ga_2O_3/Al_2O_3 interface and in the dielectric [6]. Through an analytical model, they quantified how trap density varies with depth into the Al_2O_3. The main finding was that before electrical stress, traps were relatively uniformly distributed in the dielectric, but after applying a positive bias, the trap density became depth-dependent, with notable increase in traps closer to the interface [6]. This indicates that stress can activate or create traps, possibly via defect generation or oxygen vacancy migration near the interface.

Some studies have reported findings of deep-level noise in MOVPE-grown β-Ga_2O_3 layers. Their measurements revealed that the low-frequency noise spectrum consisted of both the continuous $1/f$ background and well-resolved g-r noise components [7]. The presence of distinct generation recombination noise peaks is evidence of discrete deep levels in the bandgap of Ga_2O_3 that can trap and release carriers at characteristic time scales. By analyzing the Lorentzian components, the authors could estimate the capture/emission time constants and densities of specific trap levels. This study underscored that even in nominally high-quality epitaxial Ga_2O_3, there exist deep traps that dominate noise at certain frequencies. The derived Hooge parameter for $1/f$ noise in their films was relatively low, indicating decent material quality, but the g-r signals pointed to deep donor or acceptor levels that align with known Ga_2O_3 deep defects. In essence, this work provided an early identification of trap signatures in Ga_2O_3, showing that flicker noise analysis can serve as a spectroscopic tool for deep levels in this UWBG semiconductor [7].

Low frequency noise investigations of Ga_2O_3 Schottky barrier diodes, including alloyed Al and Ga_2O_3 structures observed that the diodes' noise spectral density exhibited the classic $1/f$ dependence at low biases, but at intermediate current levels, pronounced Lorentzian peaks appeared in the spectrum [8]. These bulges were accompanied by random telegraph noise in the time-domain, directly linking them to two-level fluctuation processes [8]. The random telegraph signal noise became more evident in a certain biasing range and was correlated with the onset of depletion region traps becoming active. The authors attributed these Lorentzian components to defects near the Schottky interface that was likely deep traps at or near the metal/Ga_2O_3 junction that can modulate the barrier height locally [8]. Such traps might be associated with interface states or impurities diffused from the contact. The normalized noise amplitude in their β-$(Al,Ga)_2O_3$ diodes was around 10^{-12} $\mathrm{cm}^2/\mathrm{Hz}$ at 10 Hz [8], which is on par with other UWBG diode materials. This work is significant because it demonstrates how low-frequency noise can be used to assess material and interface quality in Ga_2O_3 power diodes [8]. A low flicker noise floor implies low defect densities, whereas the presence of RTS signals alerts us to specific trap levels that could induce reliability issues [8].

Previous research of low frequency noise in Ga_2O_3 layers revealed trap states in these materials. Fewer studies have investigated how etched structures in these materials influence

Lorentzian noise components. Therefore, comparing 20 nm and 30 nm etching in samples could help reveal additional information about the location of active trap centers. Either they are near the newly etched surface, sidewall or even deeper regions in the semiconductor layer.

2. Low-frequency noise measurement methodology

2.1 Experimental setup

This research paper covers the investigation of multiple β-Ga_2O_3 semiconductor samples. The current-voltage characteristic of this semiconductor layer was measured at room temperature (293 K). Also, the voltage noise spectral density dependences on frequency of the layers were measured at voltages ranging from: $-2 \div 2$ V. The cross-section correlation of the noise signal was measured to determine substrate current leakage. The general measurement scheme is presented in (Fig. 1).

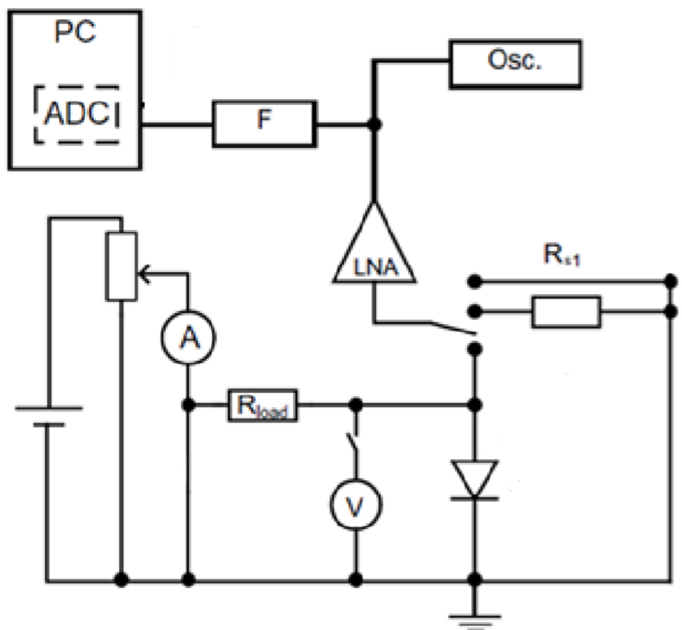

Fig. 1. β-Ga_2O_3 sample measurement principal schematic.

For β-Ga_2O_3 measurements, the circuit uses a direct current source that is a 12 V battery, the current change in the channel is changed with a potentiometer to the maximum value before having to change the load resistance R_{load} to a higher value. R_{load} is a resistors array that is connected in series, which consists of 11 different resistors $R_{1 \div 11} = 740 \div {\sim}3{,}3 \cdot 10^6\ \Omega$.

The circuit's electrical signal is connected to an oscilloscope, after first amplifying the signal using a low-noise amplifier –(LNA), which has its own separate load resistor $R_{et} = 4{,}6$ kΩ. This analog signal from the amplifier is sent to a National Instruments analogue to digital PCI-6115, which converts it into a digital signal. Digital spectral noise density calculations are performed using a program that computes the Fast Fourier Transfrom and represents spectral density as a function of frequency, whilst also averaging the spectra.

With the program, certain physical parameters are measured, S_D- the total diode and measurement system, S_T - shortened measurement system, and S_R- reference load resistor voltage noise fluctuation spectral density in a wide frequency range: $-\ f = 10\ \div 20\ \times 10^3$ Hz. The temperature measured in the shielded laboratory was 293 K.

First, the current voltage characteristics were measured in the range: $-\ 2 \div 2$ V for all β-Ga_2O_3 samples and channel lengths. These measurements help determine if the dependence is ohmic or nonlinear and approximate sample resistance at different biasing voltages. During the experiment, electric noise was measured, which represents the voltage spectral fluctuations in the β-Ga_2O_3. These measurements were also done while changing the samples temperature in the range from 77 K to 293 K. The temperature was measured using a PT-100, a 100 Ω platinum resistor.

2.2 β-Ga_2O_3 samples

In this work, two β-Ga_2O_3-based samples were investigated: TO-E6 and TO-D2-06. Both samples had rectangular-shaped contacts with varying spacings, allowing the investigation of low frequency noise dependency on channel length.

Sample TO-E6

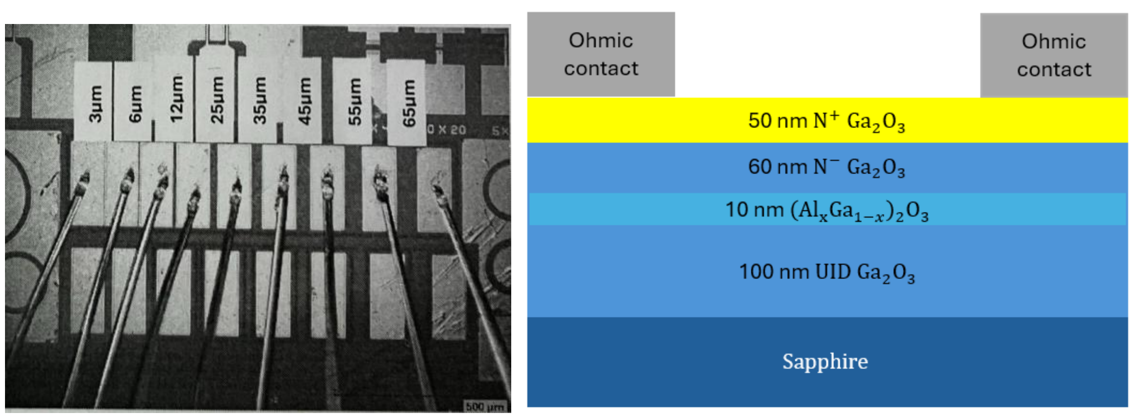

Fig. 2 TO-E6 Gallium oxide semiconductor structure.

The first investigated sample was TO-E6. This sample consisted of a β-Ga_2O_3-based heterostructure grown on a sapphire substrate. The structure diagram is shown in Fig. 2: the layer stack consisted of a 100 nm unintentionally doped Ga_2O_3 layer, a 10 nm $(AlGa)_2O_3$layer, a

60 nm n-type Ga_2O_3 layer, and a 50 nm heavily doped n^+- Ga_2O_3 contact layer. Ohmic contacts were formed on top of the structure.

In this sample, the n^+-Ga_2O_3 contact layer was not removed in the region between the ohmic contacts. Therefore, the main current path between the contacts was expected to pass through the highly conductive n^+-Ga_2O_3 layer. This sample was used as a reference structure without intentional recess etching as to take the part of an undamaged structure. The spacing between contacts on the sample was: 3, 6, 12, 25, 35, 45, 55, 65 μm, giving 8 different lengths of gallium oxide that were investigated.

Sample TO-D2-06

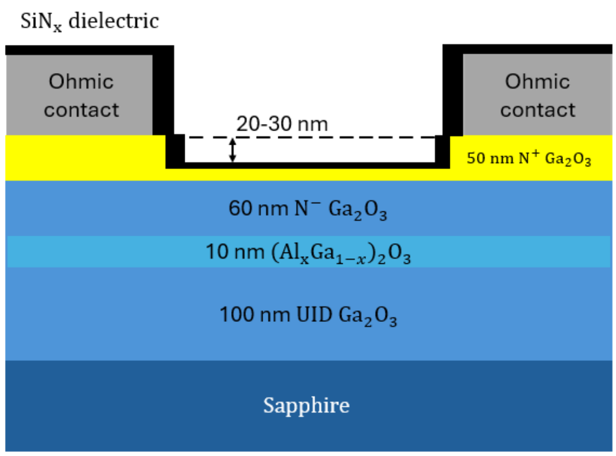

Fig. 3 Gallium oxide sample with rectangular chemical etching.

The second investigated sample was TO-D2-06. This sample also consisted of a β-Ga_2O_3-based layered structure on a sapphire substrate, but unlike TO-E6, the highly doped n^+-Ga_2O_3 contact layer was partially removed between the ohmic contacts. The layer structure consisted of a 1000 nm unintentionally doped Ga_2O_3 layer, a 70 nm n-type Ga_2O_3 layer, and a 50 nm n^+-Ga_2O_3 contact layer. A SiN_x dielectric layer was also present above the structure.

The purpose of the recess etching was to partially remove the $n^+Ga_2O_3$ contact layer in the active region between the ohmic contacts. The sample contained two etched regions: one side was etched by 20 nm, while the other side was etched to a depth of 30 nm. Therefore, TO-D2-06 allowed comparison between two different rectangular recess depths on the same sample structure. The contact spacings for the etched structures:

Table 1. TO-D2-06 sample contact spacings and etched structure length.

Contact spacing, μm	12.5	15	20	25	30	35	40
Etched length, μm	6.5	9	14	19	24	29	34

The main difference between TO-E6 and TO-D2-06 is the treatment of the highly doped n^+-Ga_2O_3 layer in the active region between contacts. In TO-E6, this layer remained unetched, so the measured current was expected to flow mainly through the n^+- Ga_2O_3 layer. In TO-D2-06, the n^+-Ga_2O_3 layer was partially removed by recess etching, forcing the current path to be more strongly influenced by the lower-doped Ga_2O_3 layers and by the etched surface region.

This difference is important for interpreting the low-frequency noise measurements. The unetched TO-E6 sample can be treated as a reference structure dominated by the conductive contact layer, while TO-D2-06 is more sensitive to surface and near-surface defects introduced or modified by the etching process.

3. Results

3.1 Current-voltage characteristic of the investigated Ga_2O_3 layers

The current-voltage characteristics were measured first to evaluate the behavior of β-Ga_2O_3 structures. There were two samples: TO-E6 and TO-D2-06. TO-E6 was a plain rectangular structure with an undamaged n^+-Ga_2O_3 layer. And the secondary sample TO-D2-06 had regions that were partially removed by recess etching to two finite depths of 20 and 30 nm.

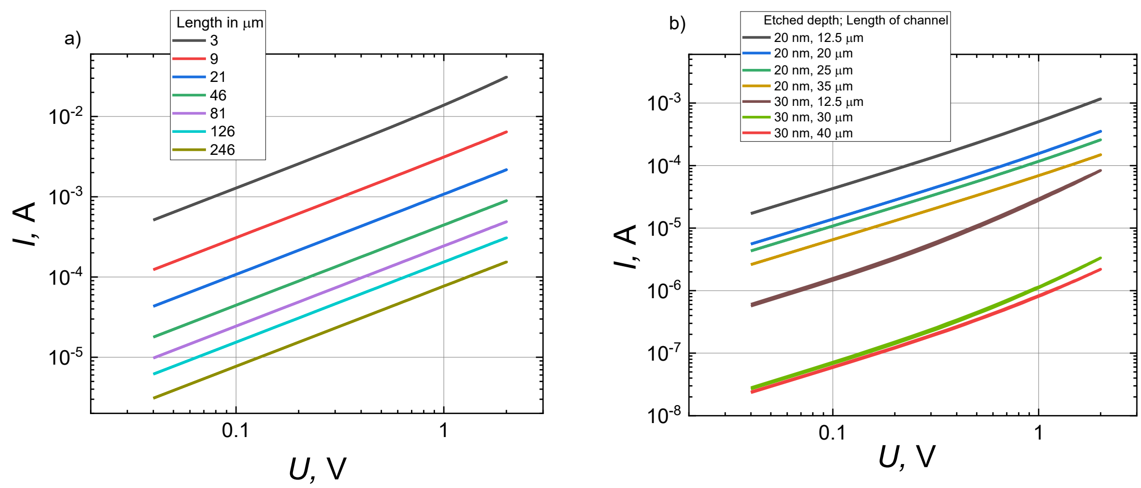

Fig. 4 a) Current-voltage characteristic of unetched β-Ga_2O_3; b) current-voltage characteristic of etched β-Ga_2O_3 samples.

The current voltage characteristics of the investigated β-Ga_2O_3 of the unetched sample are shown in Fig. 4 (a). The measurements were made for all the different channel lengths. The increase of current was linear from applied voltage in all the sample lengths. The shortest channels had the largest current, indicating longer samples had a larger resistance. The current-voltage of the etched sample is shown in Fig. 4 (b). The measurements were done in two groups: one group of 20 nm depth and the other group of 30 nm. The partial removal of the negatively doped layer resulted in lower currents. This implies that the resistance of the etched sample was larger. Comparing the two differently etched regions shows that a deeper recess gives a stronger reduction in current. This is caused by the reduced cross-sectional area of the conductive channel.

After the current-voltage characteristic measurements the resistance-voltage dependence was calculated to evaluate resistance changes when changing the biasing voltage from -2 to +2 V. These dependences for the first sample TO-E6 are shown in Fig. 5 (a). This sample had almost constant resistance over the measured voltages. The channel resistance increased with longer samples this is shown in Table 2.

The resistance-voltage dependence of the etched sample TO-D2-06 is shown in Fig. 5 (b). This sample has a considerably larger resistance up to 3 orders of magnitude. Resistance of etched structures had a stronger dependence on voltage. Deeper 30 nm recesses contributed to significantly larger resistances, the 10 nm of etching results to about 2 orders of resistance change. From this behavior it can be said that the partial removal of the n^+-Ga_2O_3 layer increases the effect of lower doped regions.

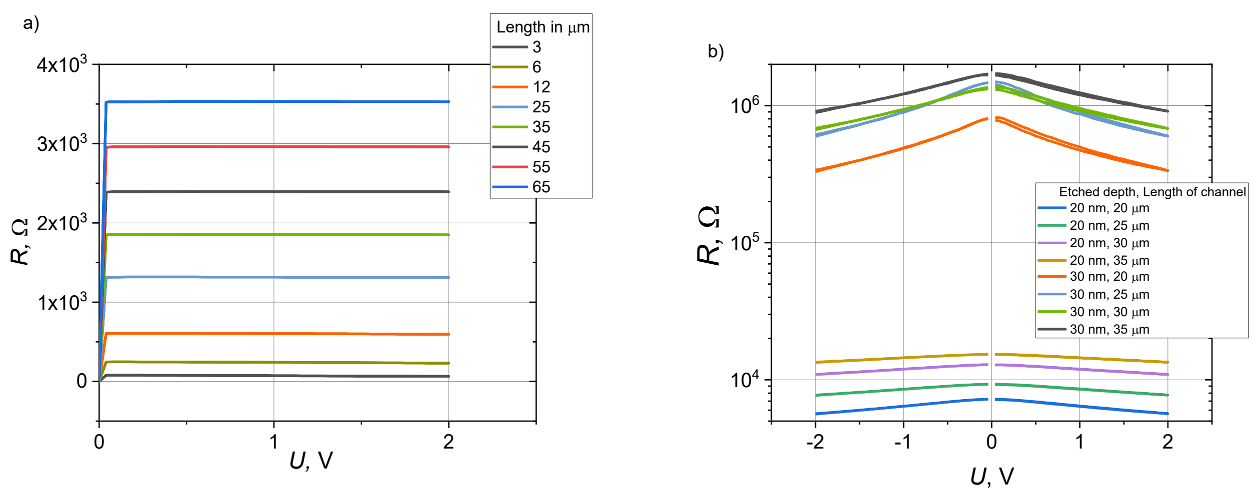

Fig. 5 Resistance-voltage dependences of β-Ga_2O_3 samples: (a) unetched TO-E6 sample with different channel lengths; (b) TO-D2-06 sample with 20 nm and 30 nm etched regions.

Table 2. β-Ga_2O_3 sample length resistances of unetched and etched samples at 1 V bias.

Length of unetched sample, µm		**3**	**6**	**12**	**25**	**35**	**45**	**55**	**65**
R, kΩ		0,08	0,25	0,6	1,3	1,8	2,4	2,9	3,5
Length of etched sample, µm		**12,5**	**15**	**20**	**25**	**30**	**35**	**40**	-
20 nm etched depth	*R,* kΩ	1,97	3,8	6,4	8,5	11,9	14,4	16,8	-
30 nm etched depth	*R,* kΩ	33,9	93,3	-	472	870	916	1198	-

3.2 Voltage noise measurements

Voltage noise spectral density measurements were performed to evaluate the low-frequency noise behavior of the investigated β-Ga_2O_3 samples. The voltage noise spectral density S_U was measured across a frequency range of 10 Hz to 20 kHz. Measurements were done for both the unetched TO-E6 sample and the recessed TO-D2-06 sample that had 20 nm and 30 nm depth regions. First, the noise spectra of the unetched sample were measured at zero applied voltage. The spectra are shown in Fig. 6.

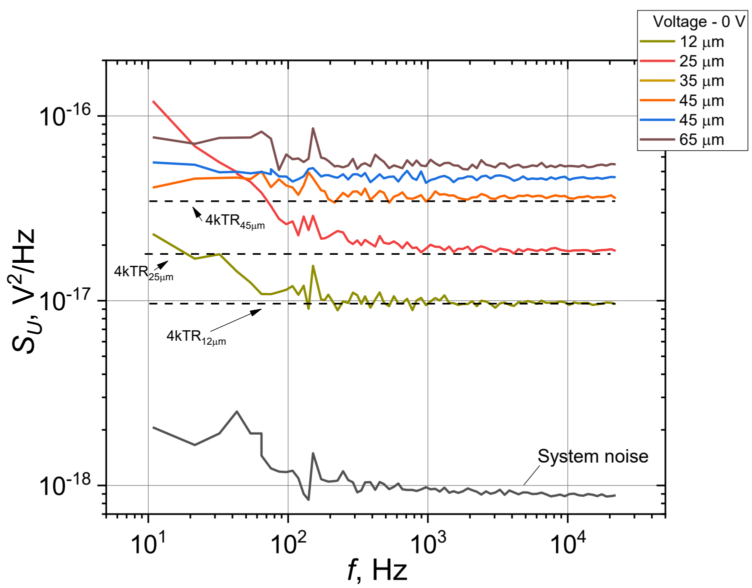

Fig. 6. Voltage noise spectral density of TO-E6 at 0 V, 293 K.

Figure 6 portrays the voltage noise spectral density $S_U(f)$ of the unetched TO-E6 sample at 0 V across multiple channel lengths. The system noise level is shown to confirm that the measured data is above the measurement floor of the system. At low bias the spectra appear to be the consequence of thermal noise of the samples. Thermal noise is proportional to the resistance of the sample $S_U = 4k_B TR$. Longer channels have a larger resistance resulting in the increase of overall noise level.

After measuring at zero bias, voltage noise spectra of the TO-E6 sample were measured under applied bias voltages of 0,1 V, 0,5 V, 1 V, 2 V. These results are shown in Fig. 7.

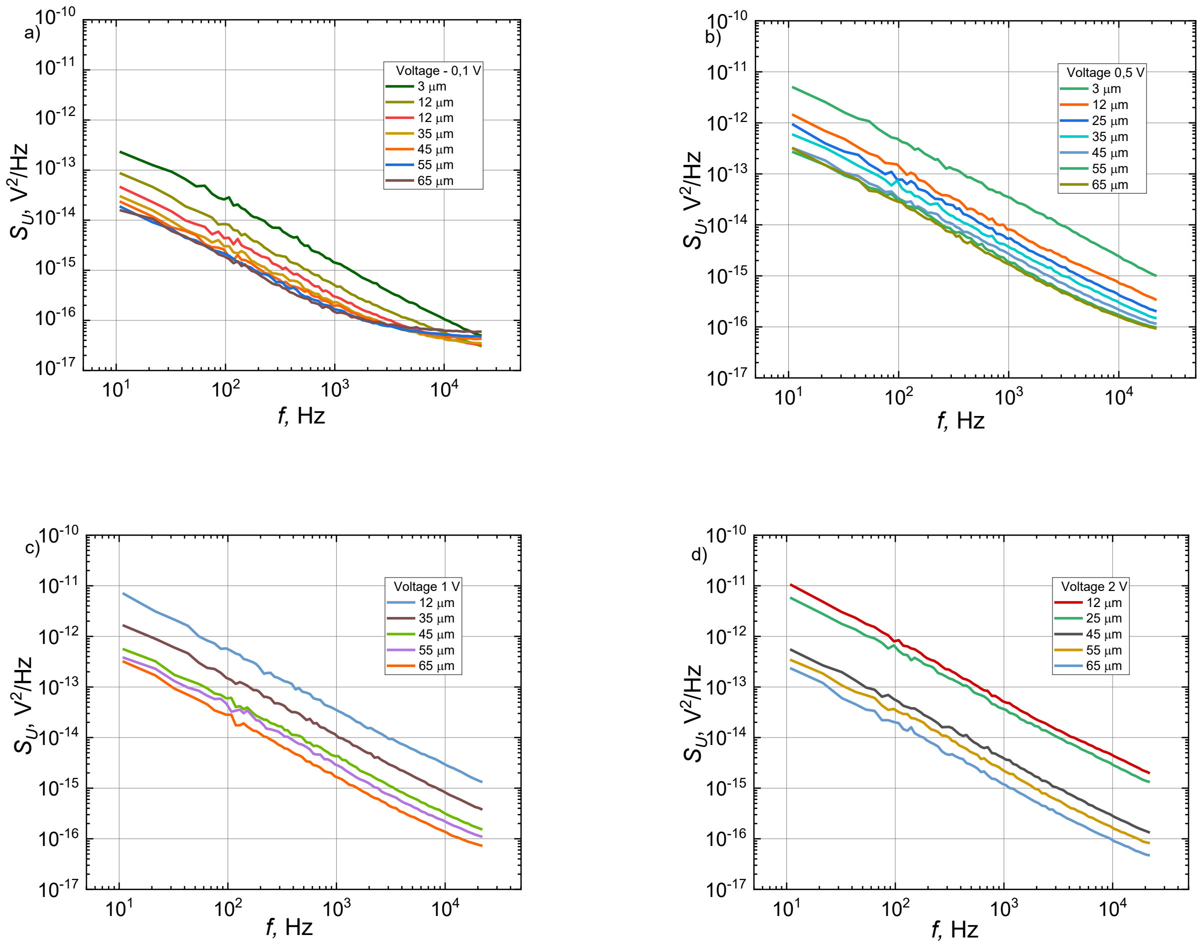

Fig. 7. Sample voltage noise spectral densities of the unetched sample: a) 0,1 V b) 0,5 V c) 1 V d) 2 V at 293 K.

Figure 7 a) through d) show that applying voltage significantly increases low-frequency noise level in comparison with zero biasing conditions that were shown in Fig. 6. For all of the investigated voltages the resulting spectra followed a $1/f^{\alpha}$ dependence. Flicker noise is the dominant noise component in all of the channels except at lower biasing conditions of 0,1 V (Fig. 7. a)). And at higher frequencies of about 10 kHz the spectra reach the thermal noise threshold. The overall trend was as follows, the shorter samples exhibited larger noise spectra values. Longer channels have more contributing generation-recombination centers that destructively interfere with one another. This may be a result of a reduction of noise contribution of individual defects.

The voltage noise spectral densities of the etched TO-D2-06 sample with etched depths of 20 nm and 30 nm are shown in Fig. 8. a) through f).

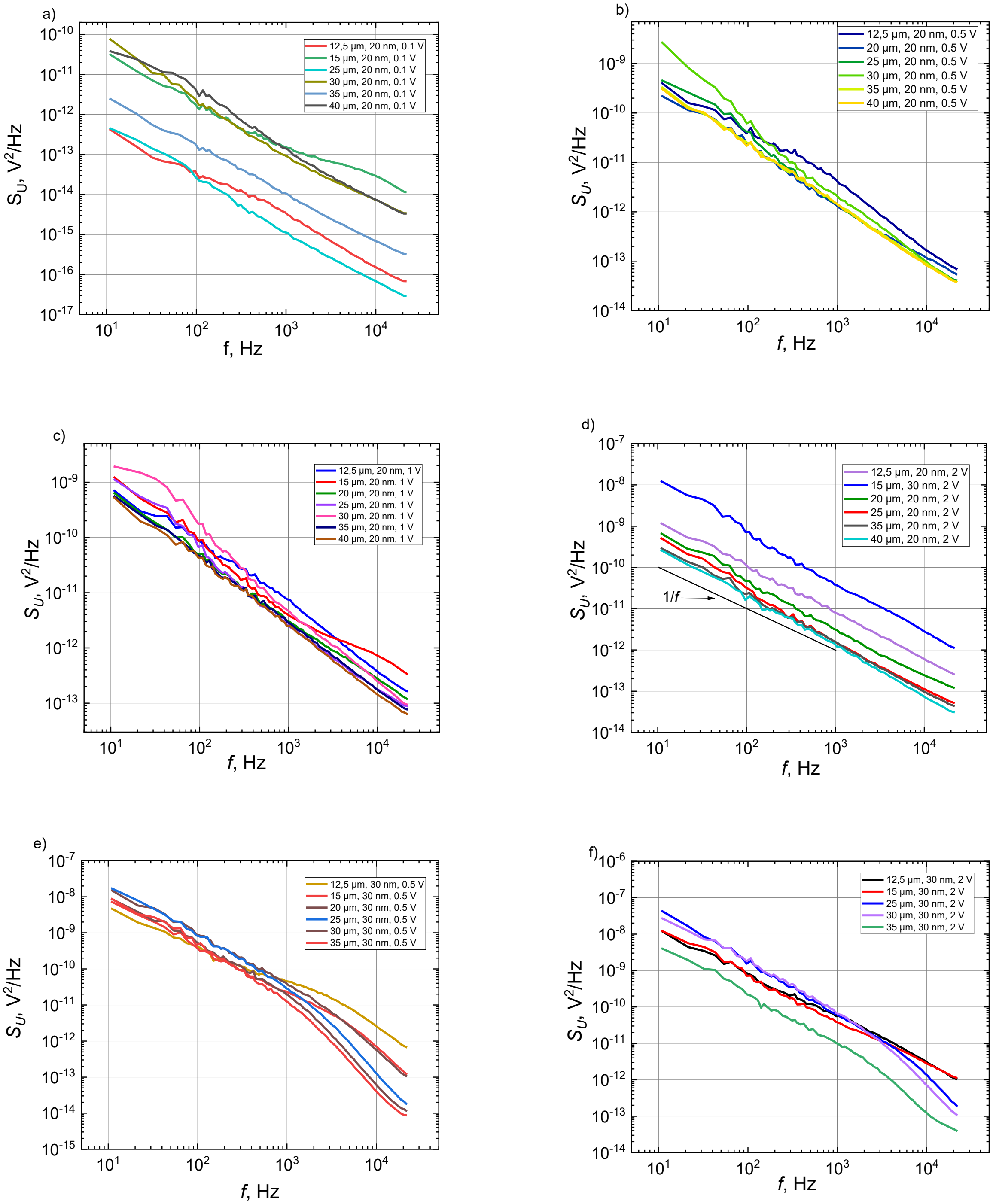

Fig. 8 TO-D2-06 sample voltage noise spectral densities at 293 K temperature for the sample with 20 nm etched depth: a) 0,1 V b) 0,5 V c) 1 V d) 2 V and for the 30 nm etched depth: e) 0,5 V f) 2V.

Most of the spectra exhibit a dependence proportional to $1/f^{\alpha}$. This indicates flicker type fluctuations in the measured noise. This occurs in spectra that do not have a singular dominant trap relaxation center. Comparing the unetched sample TO-E6 to the etched sample TO-D2-06, spectra show a significant increase in absolute noise level that is approximately two orders of magnitude larger under the same biasing conditions and similar channel lengths.

Comparing the 20 nm and 30 nm etched samples showcases that deeper recesses produce a higher noise level, which can be explained by that removal of n^{+}-Ga_2O_3 layer increases the contribution of lower doped regions.

In addition to the dominant flicker noise, several spectra appear to have Lorentzian like spectra components. They characterize the generation-recombination noise that is caused by trap centers at defined characteristic frequencies. Because these spectra appear only in the recessed samples, they may be the result of surface or near-surface states which were introduced during etching. The exact origin and values of these traps cannot be assigned from room temperature measurements and must be discussed together with temperature-dependent measurements.

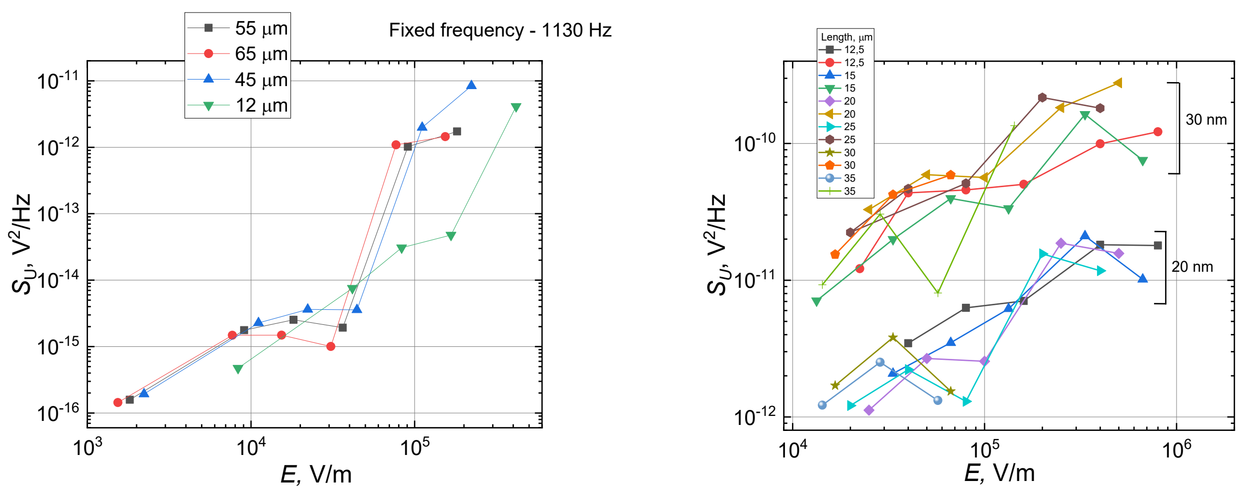

Fig. 9. Noise spectral density dependence on electric field strength: a) TO-E6 samples b) TO-D2-06 sample at fixed frequency of 1130 Hz.

Figure 9 shows the dependence of voltage noise spectral density on electric field strength E that was calculated by dividing voltage by channel length, S_U was selected at a fixed frequency of 1130 Hz.

The unetched TO-E6 samples, that is shown in Fig. 9 a), voltage noise spectral density initially increases with increasing electric field with a slight decrease at 20-30 kV/m. Afterwards, the voltage noise spectral density sharply rises at higher electric field values. Voltage noise increased from ~10^{-16} to 10^{-11} V^2/Hz. Higher electric field values strongly suggest that carrier fluctuations increase in the conductive n^+-Ga_2O_3 layer.

The etched TO-D2-06 sample that is show in Fig. 9 b) also showcases and increase of S_U with the increase of electric field. The voltage noise spectral density for the 20 nm samples ranged from ~10^{-12} to 10^{-11} V^2/Hz, and the 30 nm samples had a range of ~10^{-11} to 10^{-10} V^2/Hz. Comparing the samples, it is seen that the magnitude of noise in etched samples is larger by about 4 orders of magnitude for the 20 nm etching depth and 5 order of magnitude for the 30 nm depth sample when comparing to the unetched sample TO-E6 at lower electric field values of 1 ~20 kV/m.

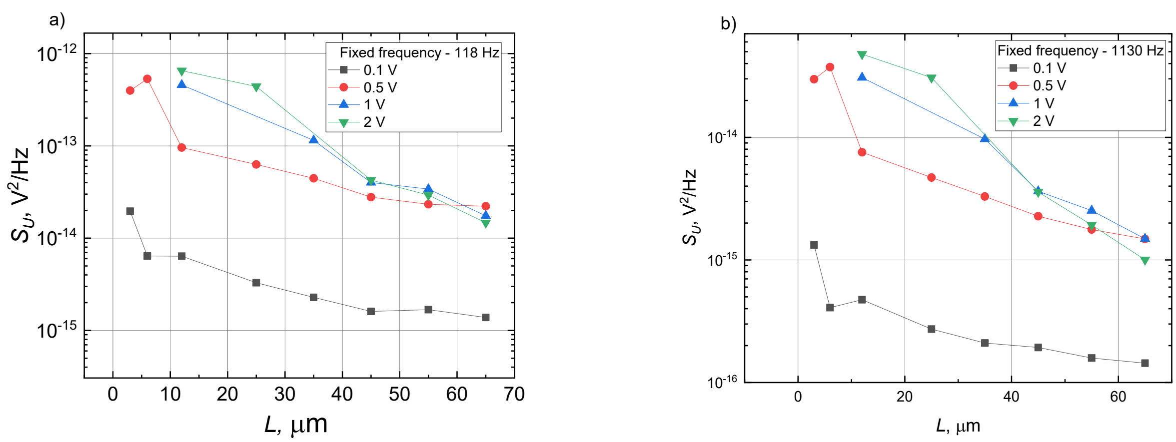

Fig. 10. TO-E6 sample voltage spectral noise density dependence on channel length at fixed frequencies: a) 118 Hz b) 1130 Hz.

Figure 10 illustrates the dependence of the voltage noise spectral density S_U on channel length L for various applied bias voltages, measured at a fixed frequencies of 118 Hz and 1130 Hz. The data include results for 0,1 V, 0,5 V, 1 V, and 2 V bias voltages. This graph shows that there is an inverse relationship between voltage spectral noise density and channel length of gallium oxide layers. This could be explained by the larger electric field values in shorter channels.

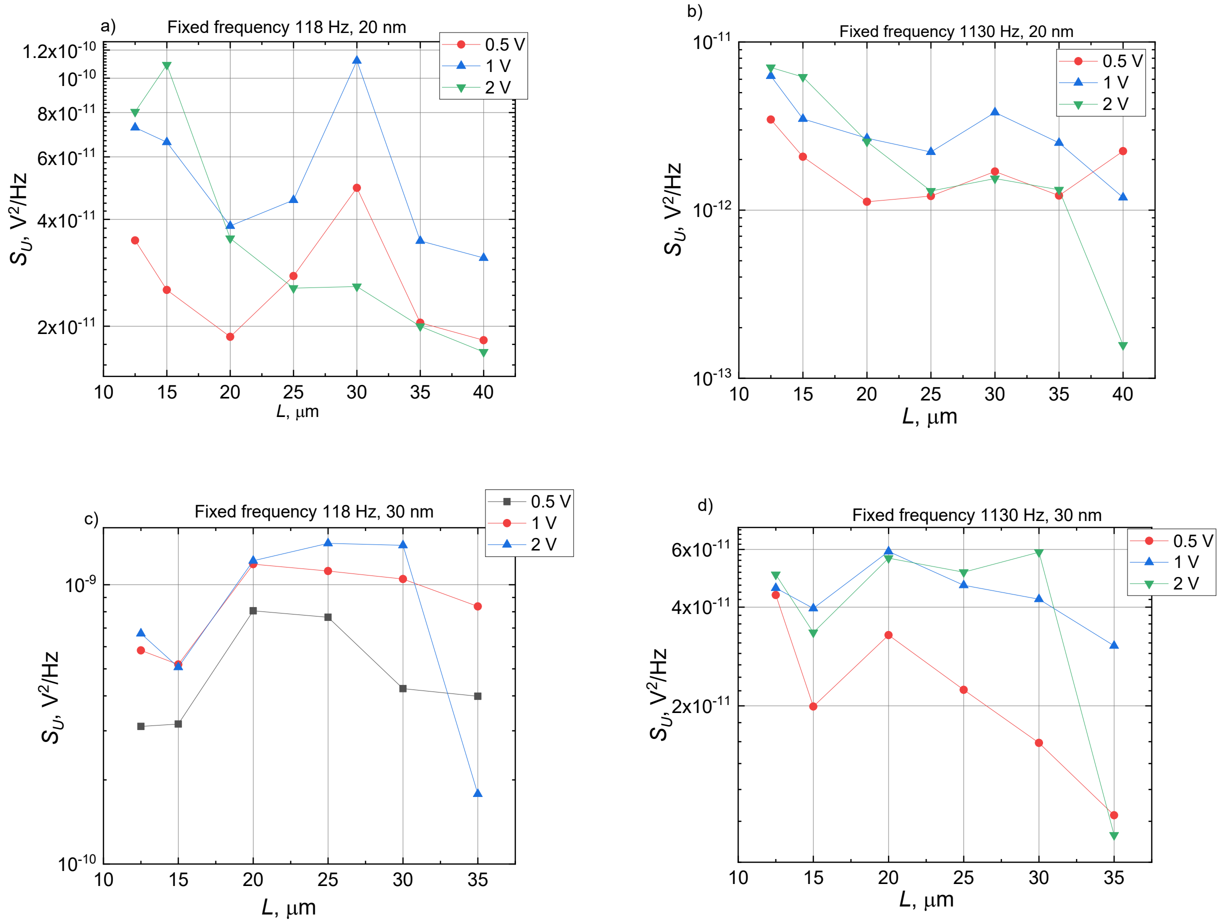

Fig. 11 TO-D2-06 sample voltage spectral noise density dependence on channel length at fixed frequencies: a) 118 Hz b) 1130 Hz for the 20 nm samples, c) 118 Hz d) 1130 Hz for the 30 nm samples.

Figure 11 shows the voltage noise spectral density dependence on channel length. For the 20 nm etched sample the dependence is shown in Fig. 11 a), b), voltage noise spectral density at 2 V decreases with channel length increase. Exceptions occur at 25 μm and 30 μm where noise level sharply rises, this could be explained by a change in defect density or current path in those specific channel lengths.

The voltage noise dependence on length for the 30 nm etched sample are shown in Fig. 11 c), d), voltage noise spectral density is about one order of magnitude larger than in the 20 nm sample at both frequencies. Also, the deeper etched sample has an irregular dependence from length. At 1130 Hz, the behavior is also irregular, however S_U starts decreasing from 20 μm to longer lengths.

Comparing the two groups of samples, deeper 30 nm etching increases the overall magnitude of voltage noise. Deeper etching may increase the effect of lower doped regions in the material which changes dominant noise contributions.

3.3 Correlation measurements

Table 3. Noise spectral density correlation measurements for different samples measured at the same time.

Principle schematic	Voltage top sample, V	Voltage bottom sample, V	Correlation between layer noise spectra densities
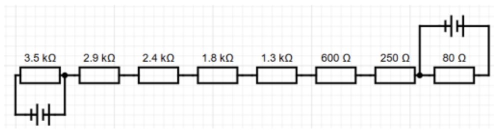	0,16	0,16	1,8 %
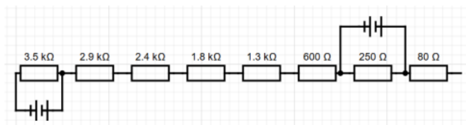	0,18	0,18	0,22 %
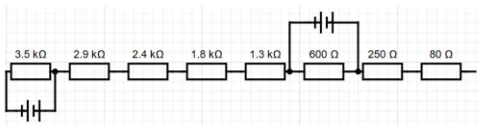	0,17	0,17	1,6 %
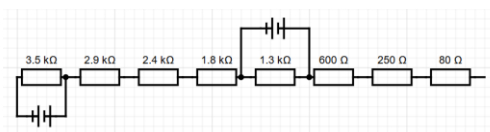	0,36	0,36	0,13 %
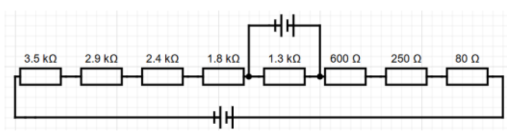	0,24	1,7	97,2 %
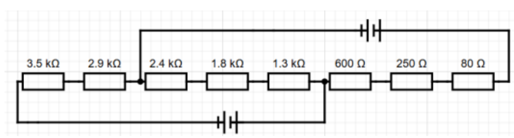	1,4	0,77	81,3 %

To evaluate independence and cross-interference between voltage noise sources in the Ga_2O_3 structure of the TO-E6 unetched sample, correlation measurements were performed. These measurements were performed using a two-channel setup. As shown in Table 2, correlation analysis was conducted between spectral noise densities of adjacent and non-adjacent channels.

The results show a clear trend that physically separated segments have little to no significant correlation, with values typically below 2 %. This indicates that noise in these channels is statistically independent, confirming minimal current is shared across the substrate.

In comparison, configurations where the measurement regions overlap or are within one another show strong correlation, with values reaching 97,2% and 81,3%, respectively. These high correlations confirm that overlapping channels share a common conduction path, the result being highly correlated noise fluctuations.

3.4 Temperature dependence measurements

Temperature dependent voltage noise spectral density measurements were done to evaluate if low frequency noise components are related to an activated trap process. The measurements were done on two channels of TO-D2-06, both samples were 15 µm in length and had different etching depths of 20 nm and 30 nm.

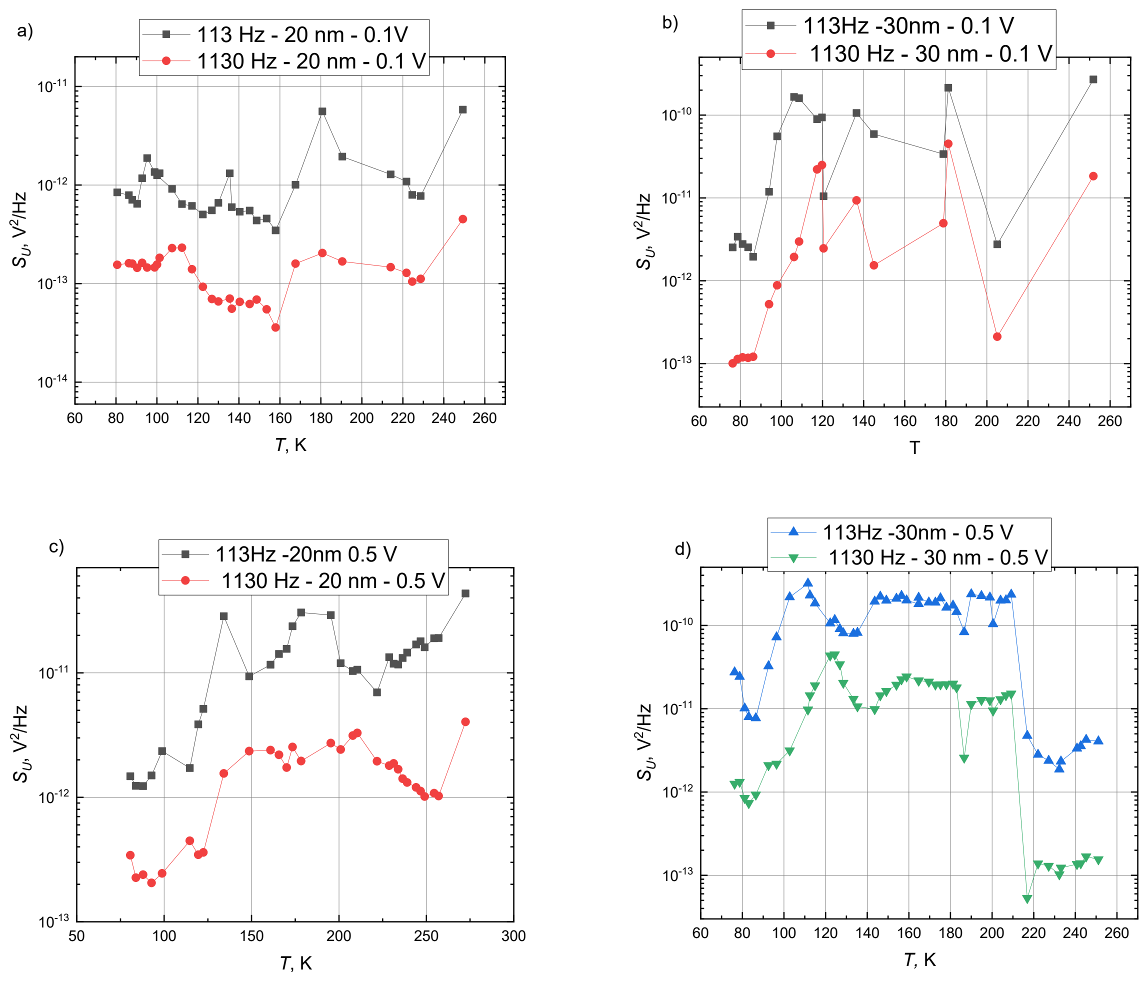

Fig. 12 Voltage noise spectral density dependence on temperature at fixed voltage and frequency values: a) 20 nm at 113 Hz and 1130 Hz with 0,1 V bias, b) 30 nm at 113 Hz and 1130 Hz with 0,1 V bias, c) 20 nm at 113 Hz and 1130 Hz with 0,5 V bias, d) 30 nm at 113 Hz and 1130 Hz with 0,5 V bias.

Figure 12 shows fixed-frequency noise spectra temperature dependence. The 20 nm and 30 nm etched regions at 0,1 V in Fig. 12 a) and b), have non-monotonic responses to temperature changes. Which could be explained by a change in dominant trap processes due to a change in sample temperature. In Fig. 12 c) the 20 nm etched sample at 0,5 V biasing showcased an increase of voltage noise spectral density up until 200 K for both fixed frequencies. The dependence of S_U for the 30 nm sample at 0,5 V is shown in Fig. 12 d), where the signal noise increases from 80 K to 110 ~120 K afterwards remaining relatively constant. When the sample reaches 216 K signal noise drastically decreases by about two orders of magnitude. This could be the result of a dominant trap center change rather than a direct reduction of all noise.

To analyze the Lorentzian spectra that became prominent in the voltage noise spectral densities, the result was sorted into groups of Lorentzian type spectra that represent the same trap-center which characteristic frequency shifts over different temperatures. One of the groups is shown in Fig. 14.

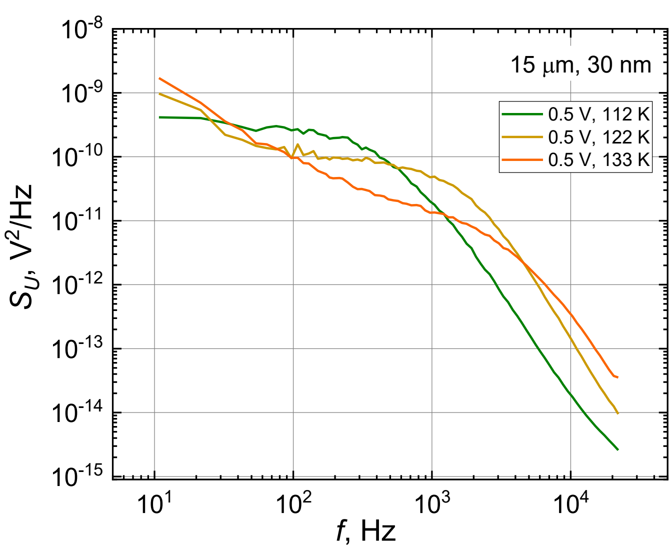

Fig. 13. A group of Lorentzian-type spectra plateauing at different characteristic frequencies.

The goal of modelling the spectra is to achieve values of the trap-center relaxation time - τ. The graphs shown in Fig. 13. are approximated to find their characteristic frequencies. To achieve this, a fitting function is used:

$$S_U(f) = \frac{A}{f} + \frac{B}{f^{\alpha}} + \frac{L\tau}{1 + (2\pi f\tau)^2} + 4k_{\mathrm{B}}TR, \tag{3.1}$$

where - A, B, L, α are coefficients and τ is the relaxation time of the trap center. Fitting the spectra in Fig. 13. allows the decomposition of the spectra into their components. An example graph for voltage noise spectral density fitting is given in Fig. 14.

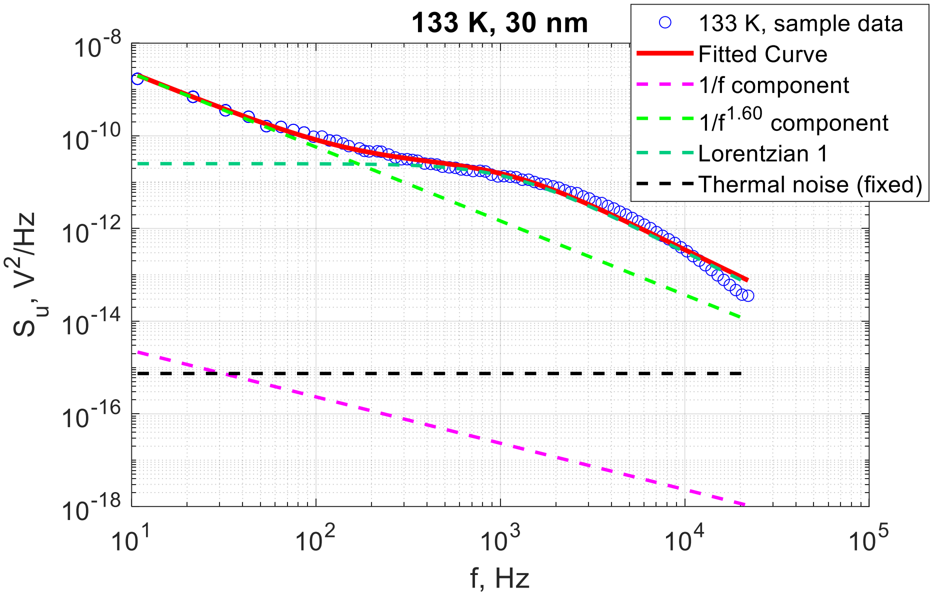

Fig. 14. Voltage noise spectral density fitting of TO-D2-06 15 μm, 30 nm etched depth.

From this, fitting multiple τ values are acquired which allows the approximation of the activation energy of the trap-centres. The calculated activation energies were $0{,}11 \pm 0{,}02$ eV for the 20 nm etched sample and $0{,}13 \pm 0{,}01$ eV for the 30 nm etched sample correspond to shallow trap levels close to the conduction band of Ga_2O_3. Since the activation energy changes with etched depth, these traps are most likely associated with the etched Ga_2O_3 surface/sidewall region or near-surface defect states introduced or exposed by etching. Referencing the correlation measurements the Ga_2O_3/sapphire interface should not have any impact on trap states because there is no significant current through the sapphire layer. Similar results have been shown in various research where activation energies were similar [19][20].

Conclusion

1. Investigation of low-frequency voltage noise characteristics of β-Ga_2O_3 layers on heterostructures have confirmed dominant $1/f$ noise behaviour above 0,1 V for the unetched sample with noise magnitudes increasing from ~10^{-16} to 10^{-13} V^2/Hz as bias increased. Shorter channels exhibited higher noise level, reaching $S_U = 3{,}6 \times 10^{-15}\ \mathrm{V^2/Hz}$ for 45 µm sample at 20 kV/m. The etched samples exhibited $1/f^{\alpha}$ and Lorentzian type components above 0,1 V voltage with noise magnitude ranging from ~10^{-16} to 10^{-9} V^2/Hz, and with noise intensity of 30 nm etched layers exceeding the 20 nm ones.
2. In the unetched sample noise level decreased with increasing length, while the etched samples showed a nonlinear response to change in length for both 20 nm and 30 nm etched layers, what shows that etching introduces additional noise sources possibly related to the surface, and the intensity is no longer directly related to the layer resistance.
3. Correlation tests on the unetched sample revealed <2% noise correlation between isolated segments, and >80% correlation in overlapping structures confirming that current does not flow through the sapphire substrate.
4. Low frequency noise spectroscopy revealed the presence of discrete trap centers with an activation energy of 0,11 eV for the 20 nm recessed structure and 0,13 eV for the 30 nm recessed structure that are the result of surface/interface defects in the semiconductor material.

Bibliography

[1] A.-C. Liu, C.-H. Hsieh, C. Langpoklakpam, K. J. Singh, W.-C. Lee, Y.-K. Hsiao, R.-H. Horng, H.-C. Kuo, and C.-C. Tu, "State-of-the-Art β-Ga_2O_3 Field-Effect Transistors for Power Electronics," *ACS Omega*, vol. 7, no. 41, pp. 36070–36091, (2022).

[2] N. S. Jamwal and A. Kiani, "Gallium Oxide Nanostructures: A Review of Synthesis, Properties and Applications," *Nanomaterials*, 12(12), 2061 (2022).

[3] A. J. Green *et al.*, "β-Ga_2O_3 Power Electronics," *APL Materials*, 10, 029201 (2022).

[4] L. K. J. Vandamme, "Noise as a diagnostic tool for quality and reliability of electronic devices", *IEEE Transactions on Electron Devices*, 41(11), 2176-2187 (1994).

[5] Tang, M., Liu, L., Jia, C., Wu, S., Lee, Y. J., Wang, G., Ma, Y., Jeon, D. W., Park, J. H., Zhang, Y., Yi, X., Wang, Y., Wang, J., & Li, J. Low frequency noise in β-Ga_2O_3 based nanoelectronic devices. *Applied Physics Letters*, *123*(1), Article 013506, (2023).

[6] H. Bae, G. B. Lee, J. Yoo, et al., "Low-frequency noise characterization of positive bias stress effect on the spatial distribution of trap in β-Ga_2O_3 FinFET," *Solid-State Electronics*, 215, 108882, (2024).

[7] C. Golz, Z. Galazka, A. Popp, S. Bin Anooz, G. Wagner, F. Hatami, and W. T. Masselink, "Deep-level noise characterization of MOVPE-grown β-Ga_2O_3," *Applied Physics Letters* 115, 133504, (2019).

[8] S. Ghosh, D. H. Mudiyanselage, S. Rumyantsev, et al., "Low-Frequency Electronic Noise in the Aluminum Gallium Oxide Schottky Barrier Diodes," *Applied Physics Letters*, vol. 122, no. 21, Art. no. 212109, (2023).

[9] D. Guo, H. Liu, P. Li, Z. Wu, S. Wang, C. Cui, C. Li, and W. Tang, "Zero-Power-Consumption Solar-Blind Photodetector Based on β-Ga_2O_3/NSTO Heterojunction," *ACS Applied Materials & Interfaces*, (2022).

[10] S. Dhara, N. K. Kalarickal, A. Dheenan, C. Joishi, and S. Rajan, "β-Ga_2O_3 Schottky barrier diodes with 4.1 MV/cm field strength by deep plasma etching field-termination," *Applied Physics Letters*, vol. 121, no. 20, p. 203501, (2022).

[11] H. Nyquist, "Thermal agitation of electric charge in conductors", Phys. Rev., 32, 110 (1928).

[12] J.B. Johnson, "Thermal agitation of electricity in conductors", Phys. Rev., 32, 97 (1928).

[13] W. Schottky, "On spontaneous current fluctuations in various electrical conductors", J. Micro/Nanolith. MEMS MOEMS, 17, 041001, (2018).

[14] X. Chen, "On Schottky Noise and Shot Noise", arXiv preprint arXiv:1805.12207 (2018).

[15] K. H. Lundberg, “Noise Sources in Bulk CMOS,” Massachusetts Institute of Technology, Cambridge, MA, USA, Oct. (2002).

[16] V. Mitin, L. Reggiani, L. Varani, "Generation-Recombination Noise in Semiconductors", in Noise and Fluctuations Control in Electronic Devices, edited by A. Balandin, American Scientific Publishers (2002).

[17] F.N. Hooge, "1/f noise is no surface effect", Phys. Lett. A, 29, 139 (1969).

[18] V. Palenskis, Fliuktuacijos elektroninėse sistemose (Vilnius: VU, 2010) 200 p.

[19] A. Almalki, “Investigation of structural, electrical and optical properties of advanced wide bandgap semiconductor materials and devices,” Ph.D. dissertation, University of Nottingham, Nottingham, U.K., (2023).

[20] J. A. Montes, “Electronic devices based on ultra-wide bandgap AlN and β-Ga_2O_3: Device fabrication, radiation effects, and defect characterization,” Ph.D. dissertation, Arizona State University, Tempe, AZ, USA, (2021).

Santrauka

Kipras Gudeliauskas

Įvairialyčių darinių su galio oksido sluoksniu triukšminė spektroskopija

Šiame darbe buvo tirtos žemo dažnio triukšmų charakteristikos β-Ga_2O_3 puslaidininkiniuose sluoksniuose. Tyrime analizuojamas įtampos triukšmo spektrinio tankio priklausomybė nuo dažnio, įtampos ir bandinio varžos. Įtampos fliuktuacijų spektriniai tankiai buvo matuojami plačiame temperatūrų intervale 77 K-293 K, naudojant mažo triukšmo stiprintuvą ir matuojant 10 Hz-20 kHz dažnių intervale.

Kambario temperatūroje neėsdintame TO-E6 bandinyje vyravo $1/f$ ir $1/f^{\alpha}$ tipo triukšmas, kurio intensyvumas augo didinat įtampą. Bandinio varžoms didėjant stebimas triukšmų lygio žemėjimas. Trumpesnio 12 µm bandinio įtampos fliuktuacijų spektriniai tankiai buvo dvejomis eilėmis didesni nei 65 µm bandinio, kai įtampa bandinyje buvo 2 V.

Ėsdintame TO-D2-06 bandinyje triukšmų lygis buvo žymiai didesnis nei neėsdintame bandinyje. 20 nm ir 30 nm gylio ėsdinimas galio oksido struktūroje padidino įtampos fliuktuacijų spektrinį tankį. Stebėti triukšmai buvo $1/f$ ir $1/f^{\alpha}$ tipo.

Atlikti vienalaikiai koreliacijos matavimai parodė, kad atskirų bandinių sluoksnių triukšmų spektrai nekoreliavo (<2 %), o dalinai persidengiančių sluoksnių triukšmų spektrai turėjo ryškią koreliaciją (>80 %). Koreliacijos nebuvimas tarp nepersiklojančių sluoksnių reiškia, kad srovė tekėjo tik per tiriamus galio oksido sluoksnius.

Temperatūriniuose matavimuose buvo pastebėti Lorenco tipo spektrai. Analizuojant įtampos fliuktuacijų spektrinio tankio temperatūrinį kritimą, buvo modeliuoti spektrai. Radus aktyvacijos centrų relaksacijos laikus buvo apskaičiuota jų aktyvacijos energija dviem ėsdintiems bandiniams: 15 µm ilgio ir 20 nm ėsdinto bandinio energija buvo $E \approx 0{,}11$ eV, o gilesnio 30 nm ėsdinimo bandiniui or 15 µm ilgio bandiniui, energija buvo $E \approx 0{,}13$ eV. Aktyvacijos energijos yra nedidėlės, todėl tikėtina, kad jos susijusios su paviršiniais defektais puslaidininkio struktūroje.